

Revisiting the stability of circular Couette flow of shear-thinning fluids

Brahim Alibenyahia, Cécile Lemaitre, Chérif Nouar, Noureddine Ait-Messaoudene

▶ To cite this version:

Brahim Alibenyahia, Cécile Lemaitre, Chérif Nouar, Noureddine Ait-Messaoudene. Revisiting the stability of circular Couette flow of shear-thinning fluids. Journal of Non-Newtonian Fluid Mechanics, 2012, 183-184, pp.37-51. 10.1016/j.jnnfm.2012.06.002. hal-03788215

HAL Id: hal-03788215 https://cnrs.hal.science/hal-03788215

Submitted on 26 Sep 2022

HAL is a multi-disciplinary open access archive for the deposit and dissemination of scientific research documents, whether they are published or not. The documents may come from teaching and research institutions in France or abroad, or from public or private research centers. L'archive ouverte pluridisciplinaire **HAL**, est destinée au dépôt et à la diffusion de documents scientifiques de niveau recherche, publiés ou non, émanant des établissements d'enseignement et de recherche français ou étrangers, des laboratoires publics ou privés.

Revisiting the stability of circular Couette flow of shear-thinning fluids

Brahim Alibenyahia ^a , Cécile Lemaitre ^b , Chérif Nouar ^c and Noureddine Ait-Messaoudene ^{a d}

^aLApEH, Université Saad Dahleb, Blida, Algeria

^bLRGP, ENSIC, 1 rue Grandville, BP 20451, 54001 Nancy Cedex, France

^cLEMTA, UMR 7563 (CNRS), 2, avenue de la forêt de Haye, BP 160, 54504

Vandoeuvre Cedex, France

^dDepartment of Mechanical Engineering, Faculty of Engineering, University of Hail, PO Box 2440 Hail, Saudi Arabia

Abstract

Three-dimensional linear stability analysis of Couette flow between two coaxial cylinders for shear-thinning fluids with and without yield stress is performed. The outer cylinder is fixed and the inner one is rotated. Three rheological models are used: Bingham, Carreau and power-law models. Wide range of rheological, geometrical and dynamical parameters is explored. New data for the critical conditions are provided for Carreau fluid. In the axisymmetric case, it is shown that when the Reynolds number is defined using the inner-wall shear-viscosity, the shear-thinning delays the appearance of Taylor vortices, for all the fluids considered. It is shown that this delay is due to reduction in the energy exchange between the base and the perturbation and not to the modification of the viscous dissipation. In the non axisymmetric case, contrary to Caton[1], we have not found any instability.

Key words: Circular Couette flow, Shear-thinning fluid, Stability analysis.

1 Introduction

Taylor-Couette flow, the flow between two rotating coaxial cylinders that are infinitely long, is a paradigm for studies of stability and transition to turbulence of sheared Newtonian fluids. For low velocities of the cylinders, the flow is steady and purely azimuthal with $U = V(r)e_{\theta}$, where e_{θ} is the unit vector in the azimuthal direction. When the angular velocity of the inner cylinder is

increased above a certain threshold, the purely azimuthal flow becomes unstable, and a stationary axisymmetric flow characterized by the appearance of counter-rotating toroidal vortices is observed. These vortices are separated by inflow and outflow radial jets. The origin of this instability is the existence of an adverse gradient of the square of the angular momentum, $d(rV)^2/dr < 0$, that allows centrifugal forces to overcome viscous forces. Taylor-Couette flow has been the subject of numerous experimental and theoretical studies since the pioneering paper of Taylor in 1923 [2]. Higher transitions as the angular velocity of the inner cylinder is increased beyond the critical value are discussed in the review of Di Prima and Swinney [3]. For non-Newtonian fluids, there was a considerable interest in inertialess viscoelastic Taylor-Couette instability, driven by the first normal-stress difference that develops due to stretching of the polymer molecules along the curved stream lines. The purely elastic Taylor Couette instabilities, observed initially by Giesekus [4], were analyzed by Muller et al. [5], Larson et al. [6] and Shaqfeh et al. [7]. Groisman and Steinberg [8] showed experimentally that the elastic instability leads to a strong nonlinear flow transition. Thomas et al. [9] investigated the nonlinear pattern formation using three dimensional dynamical simulation.

In some industrial processes, such as in oil-well cementing, the fluids used are strongly shear-thinning and slightly viscoelastic. In order to isolate the effects of shear-thinning, it is necessary to consider non-Newtonian purely viscous fluids, i.e. fluids without elastic response and with an effective viscosity $\hat{\mu}$ decreasing nonlinearly with the shear rate $\hat{\gamma}$. Surprisingly, very few studies have been devoted to this case. In the following, we give a brief literature review relying on the main results. We choose to present them according to the most commonly used rheological model namely the power-law, Carreau and Bingham models. The last one is for shear-thinning fluid with yield stress.

For power-law fluids, Sinevic et al.[10] determined the onset of Taylor vortices by measuring the torque exerted by the fluid on the rotating inner cylinder. The results obtained by the authors for CMC solution and Carbopol solutions are reported on Fig. 1. Jastrzebski et al. [11] have determined the critical Reynolds number from a linear stability analysis. They conclude that the shear-thinning has a destabilizing effect. Lockett et al. [12] used a 2D finite element code to simulate the transient flow, and a numerical criterion is used to determine the first bifurcation. They found that the stabilizing or destabilizing effect induced by the shear-thinning behavior depends on the radius ratio $\eta = R_1/R_2$, where R_1 and R_2 are the radii of the inner and outer cylinders respectively. Escudier et al.[13] investigated the flow structure in a Taylor-Couette geometry with a radius ratio of 0.5. Axial and tangential velocity measurements were made using a laser Doppler anemometer for a an aqueous solution of Xanthan gum, which is shear-thinning and slightly viscoelastic and a Laponite/CMC blend which is shear-thinning and also thixotropic. The results reveal that the shear thinning behavior induces a significant radial shift in the location of the vortex eye towards the centrebody. In the Figure 1, we have represented the critical Reynolds number, Re_c , for the primary bifurcation, as function of the shear-thinning magnitude, given by the index n, deduced from the literature review. The existing results show rather important discrepancies. The relative difference may reach value up to 30%.

For Carreau fluids, Ashrafi and Khayat [14] and Li and Khayat [15], examined the influence of the shear-thinning on the stability of circular Couette flow in the narrow gap limit. The authors indicate that the shear-thinning tends to precipate the onset of Taylor vortex flow and to modify the shape of bifurcation branch. Coronado et al. [16] used 2D CFD code to determine the onset of instability. They conclude that if the Reynolds number is defined with the viscosity calculated at the inner rotating wall, the critical Reynolds number calculated for Newtonian fluid is a good estimation for the onset of instability for shear-thinning fluids. Nevertheless, in their study, the rheological parameters used are such that the viscosity profile departs slightly from that of a Newtonian fluid.

For Bingham fluids, Graebel [17] was the first who performed a linear stability analysis of a viscoplastic fluid flow. Using a narrow gap limit, the authors found that the yield stress has a stabilizing effect. Peng and Zhu [18] and Landry et al. [19] found that the yield stress can have a destabilizing effect in wide gap co-rotating cylinders over a limited range of Bingham numbers. An interpretation based on the exchange energy between the base flow and the perturbation is proposed.

Recently, Caton [1], indicated that for power law fluids with shear-thinning index less than 0.2, the least stable mode is non axisymmetric and consists of a large number of columnar vortices. This surprising result has not been discussed. Actually, non-axisymmetric instability in the Taylor-Couette flow was observed experimentally by Andereck et al. [20] for Newtonian fluids when the two cylinders are counter-rotating. This regime called laminar spiral flow occupies a narrow region in the stability diagram. It was also obtained by Wan Zhan-Hong et al. [21] for a fiber suspension using linear stability analysis. The rheological behavior of the suspension is described by Ericksen model and the ratio of the angular velocity of the outer cylinder to that of the inner cylinder is less than -0.6 for a radius ratio $\eta = 0.88$. It should be noted that in the case of counter-rotating cylinders, the sign of $d(rV)^2/dr$ changes within the gap.

Circular Couette flows of shear-thinning fluids are mainly characterized by a viscosity stratification in the annular space. The degree of viscosity stratification is even more significant as the fluid is more shear-thinning and the radius ratio η is small. Besides this, when an infinitesimal perturbation is imposed on the base flow, the shear-stress and the shear-rate are disturbed by $\delta \tau_{r\theta}$ and $\delta \dot{\gamma}_{r\theta}$, then the disturbance will feel the tangent viscosity $\mu_t = \delta \tau_{r\theta} / \delta \dot{\gamma}_{r\theta}$

Fig. 1. Critical Reynolds number defined by the equation (3) versus the shear-thinning index n, for power-law fluids with a radius ratio $\eta = 0.9$. (o) Sinevic *et al.* [10]; (\square) Caton [1]; (∇) Jastrebski *et al.* [11]. The error bars correspond to reading uncertainties on figures published in the literature. Here, n = 1 is the Newtonian limit and increasing shear-thinning corresponds to a decrease of n.

rather than the effective viscosity. This leads to an anisotropy of the perturbation τ' of the deviatoric-stress tensor. More details on this point are given in section 4. The objective of the present paper is to revisit the stability of shear-thinning fluid flow between two coaxial cylinders. The influence of the viscosity stratification and that of the anisotropy of τ' will be highlighted. We consider only the case where the inner cylinder is rotating and the outer is at rest. As Caton [1] suggested the existence of longitudinal rolls for strong shear-thinning fluids, we have then considered three types of perturbation: (i) axisymmetric perturbation, (ii) homogeneous perturbation in the axial direction and (iii) three dimensional perturbation. This paper is structured as follows: in section 2, the mathematical formulation of the problem is provided. Three different constitutive equations are considered: the Bingham model to represent the viscoplastic fluids, and the Carreau and power law models to represent the shear-thinning fluids without yield stress. Section 3 describes the basic flows. The influence of the rheological parameters on the viscosity stratification is discussed. In section 4, the perturbation equations are stated in the frame of the linear stability analysis. Section 5 briefly outlines the solution procedure for the eigenvalue problem that arises from the normal-mode linear stability analysis. The results are discussed in section 6. Finally, conclusions are presented in section 7.

2 Problem description

We consider the flow of an incompressible nonlinear viscous fluid between two infinitely long concentric cylinders, with inner and outer radii, \hat{R}_1 and \hat{R}_2 respectively. The inner cylinder is rotating with a constant angular velocity $\hat{\Omega}_1$ while the outer is at rest. The governing equations in dimensionless form are

$$\nabla \cdot \boldsymbol{U} = 0, \tag{1}$$

$$\frac{\partial \boldsymbol{U}}{\partial t} + Re \, \left(\boldsymbol{U} \cdot \boldsymbol{\nabla} \right) \boldsymbol{U} = -\boldsymbol{\nabla} P + \boldsymbol{\nabla} \cdot \boldsymbol{\tau}. \tag{2}$$

Here U is the velocity, P is the pressure and τ is the deviatoric extra-stress tensor. The velocity vector is of the form $U = U e_r + V e_\theta + W e_z$, where e_r , e_θ and e_z are unit vectors in the radial r, circumferential θ and axial

z directions respectively. The above equations have been nondimensionalized using the width of the annular space $\hat{d} = \hat{R}_2 - \hat{R}_1$ as the reference length scale, the velocity of the inner cylinder $\hat{\Omega}_1\hat{R}_1$ as velocity scale, $\hat{\mu}_{ref}\hat{R}_1\hat{\Omega}_1/\hat{d}$ for stresses and pressure scale and diffusion time $\hat{\rho}\,\hat{d}^2/\hat{\mu}_{ref}$ for time scale. The viscosity reference $\hat{\mu}_{ref}$ will be specified later. The Reynolds number Re is defined by

$$Re = \frac{\hat{\rho}\hat{R}_1\hat{\Omega}_1\hat{d}}{\hat{\mu}_{ref}}.$$
 (3)

The dimensionless radii of the inner and outer cylinders are respectively:

$$R_1 = \frac{\eta}{1 - \eta}$$
 and $R_2 = \frac{1}{1 - \eta}$ with $\eta = \frac{\hat{R}_1}{\hat{R}_2}$. (4)

The quantities denoted with a hat ($\hat{\cdot}$) are dimensional while quantities without ($\hat{\cdot}$) are dimensionless. In this work, we consider only the case of shear-thinning fluids, i.e., fluids for which the effective viscosity $\hat{\mu}$ decreases as the shear rate increases. For the numerical computation, we consider three different models: Bingham model (shear-thinning with a yield stress), power law model and Carreau model. After scaling, the corresponding constitutive equations read:

For Bingham model

$$\boldsymbol{\tau} = \mu \, \dot{\boldsymbol{\gamma}} = \left[\mu_p + \frac{B}{\dot{\gamma}} \right] \, \dot{\boldsymbol{\gamma}} \iff \tau > B, \tag{5}$$

$$\dot{\boldsymbol{\gamma}} = 0 \iff \tau \le B \tag{6}$$

with a Bingham number defined by

$$B = \frac{\hat{\tau}_0}{\hat{\mu}_{ref} \, \hat{R}_1 \hat{\Omega}_1 / \hat{d}},\tag{7}$$

where $\hat{\tau}_0$ is the yield stress of the fluid, $\mu_p = \hat{\mu}_p/\hat{\mu}_{ref}$ is the dimensionless plastic viscosity, $\dot{\gamma}$ and τ are respectively the second invariant of the strain-rate tensor $\dot{\gamma}$ and the deviatoric stress tensor τ . They are defined by the following relations

$$\dot{\boldsymbol{\gamma}} = \boldsymbol{\nabla} \boldsymbol{U} + \boldsymbol{\nabla} \boldsymbol{U}^T \quad ; \quad \dot{\boldsymbol{\gamma}} = \left(\frac{1}{2}\dot{\gamma}_{ij}\,\dot{\gamma}_{ij}\right)^{1/2} \quad ; \quad \boldsymbol{\tau} = \left(\frac{1}{2}\tau_{ij}\,\tau_{ij}\right)^{1/2}. \tag{8}$$

For power-law model

$$\boldsymbol{\tau} = \mu \, \dot{\boldsymbol{\gamma}} = \frac{\hat{K} \left(\hat{R}_1 \hat{\Omega} / \hat{d} \right)^{n-1}}{\hat{\mu}_{ref}} \dot{\gamma}^{n-1} \, \dot{\boldsymbol{\gamma}} \,, \tag{9}$$

where \hat{K} is the consistency and n the shear-thinning index, 0 < n < 1.

For Carreau model

$$\boldsymbol{\tau} = \mu \, \dot{\boldsymbol{\gamma}} = \mu_{\infty} + (\mu_0 - \mu_{\infty}) \left[1 + (\lambda \, \dot{\boldsymbol{\gamma}})^2 \right]^{\frac{n-1}{2}} \, \dot{\boldsymbol{\gamma}} \,, \tag{10}$$

where $\mu_{\infty} = \hat{\mu}_{\infty}/\hat{\mu}_{ref}$ is the dimensionless Newtonian plateau viscosity at high shear rates, $\mu_0 = \hat{\mu}_0/\hat{\mu}_{ref}$ is the dimensionless Newtonian plateau viscosity at low shear rates, $\lambda = \hat{\lambda}\hat{R}_1\,\hat{\Omega}_1/\hat{d}$, where $\hat{\lambda}$ is a time constant of the fluid. The dimensionless characteristic shear-rate for the onset of shear-thinning is defined by $1/\lambda$. The infinite shear viscosity, $\hat{\mu}_{\infty}$, is frequently smaller (10^{-3} to 10^{-4} times smaller) than $\hat{\mu}_0$ (Bird *et al.* [22] and Tanner [23]) and will be neglected in this study.

Concerning the reference viscosity, we have adopted in a first step, the expressions widely used in the literature which depend on the rheological model considered. For Bingham model, the reference viscosity $\hat{\mu}_{ref}$ used is the plastic viscosity $\hat{\mu}_p$. For Carreau model, the Newtonian plateau viscosity $\hat{\mu}_0$ at low shear rates is adopted as reference viscosity. For the power-law model, $\hat{\mu}_{ref} = \hat{K} \left(\hat{R}_1 \hat{\Omega}_1 / \hat{d} \right)^{n-1}$. The discussion on the choice of the reference viscosity is deferred to a later section.

3 Basic flows

The basic flow is considered stationary and axisymmetric with a purely azimuthal velocity field $U = (0, V^b(r), 0)$. The superscript b refers to the base flow. The only non zero elements of the strain rate tensor are off-diagonal $\dot{\gamma}_{r\theta}^b(r) = \dot{\gamma}_{\theta r}^b(r)$, so that the deviatoric stress tensor elements are all zero except for $\tau_{\theta\theta}^b(r) = \tau_{\theta r}^b(r) = \mu^b \dot{\gamma}_{r\theta}^b$. The momentum equations reduce to

$$0 = \frac{1}{r^2} \frac{d}{dr} \left(r^2 \tau_{r\theta}^b \right), \tag{11}$$

with the nonslip boundary conditions at the inner R_1 and outer R_2 walls

$$V^b(R_1) = 1$$
 and $V^b(R_2) = 0.$ (12)

Integration of (11) gives

$$\tau_{r\theta}^b(r) = \tau_1^b \left(\frac{R_1^2}{r^2}\right),\tag{13}$$

where $\tau_1^b = \tau_{r\theta}^b(R_1)$ is the dimensionless shear-stress at the inner wall. It is clear that $\tau_{r\theta}^b$ does not change sign in the annulus and $\left|\tau_{r\theta}^b\right|$ decreases from the inner to the outer cylinder. Using (13), the boundary conditions (12) and the rheological laws, the velocity profiles $V^b(r)$ can be easily derived.

Bingham fluid: Case where all the annular space is yielded i.e. $\left|\tau_{r\theta}^{b}(r)\right| > B$, $\forall r \in [R_1, R_2]$

$$V^{b}(r) = \frac{1}{2}R_{1}^{2}\tau_{1}^{b}r\left[\frac{1}{R_{2}^{2}} - \frac{1}{r^{2}}\right] - Br\ln\left(\frac{R_{2}}{r}\right),\tag{14}$$

with

$$\tau_1^b = \frac{2}{\eta^2 - 1} \left[\frac{1 - \eta}{\eta} - B \ln(\eta) \right]. \tag{15}$$

Using equations (5) and (14), it can be shown straightforwardly that

$$\frac{\mu^b(r)}{\mu^b(r=R_1)} = \left(\frac{R_1}{r}\right)^2 \frac{\tau_1^b + B}{(R_1/r)^2 \tau_1^b + B} \tag{16}$$

Samples of the basic velocity profiles $V^b(r)$ and of the viscosity profiles are given in Fig. 2 for radius ratio $\eta = \hat{R}_1/\hat{R}_2 = 0.5$ and different values of the Bingham number.

Bingham fluid: Case where there is an attached layer at the outer cylinder: i.e. $\exists R_0 \in]R_1, R_2[$ such that $\tau^b_{r\theta}(R_0) = B$, therefore $|\tau^b_{r\theta}(r)| < B$ for $r \in]R_0, R_2[$ and $|\tau^b_{r\theta}(r)| > B$, for $r \in [R_1, R_0[$. The radial position of the yield surface is R_0 . The no-slip condition at the external wall is replaced by $V^b(R_0) = 0$. The basic velocity in the yielded zone reads

Fig. 2. Couette flow of a Bingham fluid in the case where all the annular space is yielded for $\eta=0.5$. (a) Basic azimuthal velocity profiles: (1) B=0 Newtonian fluid; (2) B=0.5; (3) B=1.23. (b) Basic viscosity profiles: (1) B=0 Newtonian fluid; (2) B=0.5; (3) B=0.85; (4) B=1; (5) B=1.23

$$V^{b}(r) = \frac{1}{2}R_{1}^{2}\tau_{1}^{b}r\left[\frac{1}{R_{0}^{2}} - \frac{1}{r^{2}}\right] - Br\ln\left(\frac{R_{0}}{r}\right),\tag{17}$$

where τ_1^b is determined using the boundary condition $V^b(R_1) = 1$,

$$1 = -\frac{BR_1}{2} \left[1 - \frac{|\tau_1^b|}{B} + \ln\left(\frac{|\tau_1^b|}{B}\right) \right]$$
 (18)

The viscosity profil expression is identical to that given by (16)

Power-law fluid

$$V^{b}(r) = \frac{r}{R_{1}} \left[1 - \left(\frac{1}{R_{2}^{2/n}} - \frac{1}{R_{1}^{2/n}} \right)^{-1} \left(\frac{1}{r^{2/n}} - \frac{1}{R_{1}^{2/n}} \right) \right], \tag{19}$$

and

$$\frac{\mu^b(r)}{\mu^b(r=R_1)} = \left(\frac{R_1}{r}\right)^{\frac{2}{n}(n-1)}.$$
 (20)

The base state for this rheological behavior is shown in Fig. 3.

Carreau fluid

For this model, we do not have analytical expression of the velocity profile. Equation (11) combined with (10) is solved numerically using an iterative process based on the classical Newton-Raphson method. Samples of velocity and

Fig. 3. Couette flow of a power-law fluid for $\eta = 0.5$. (a) Basic azimuthal velocity profiles: (1) n = 1 Newtonian fluid; (2) n = 0.7; (3) n = 0.5; (4) n = 0.3. (b) Basic viscosity profiles: (1) n = 1 Newtonian fluid; (2) n = 0.7; (3) n = 0.5; (4) n = 0.3.

Fig. 4. Couette flow of a Carreau fluid for $\eta = 0.5$, $\lambda = 1$ and different values of the shear-thinning index. (a) Basic azimuthal velocity profiles: (1) n = 1 Newtonian fluid; (2) n = 0.7; (3) n = 0.5; (4) n = 0.3. (b) Basic viscosity profiles: (1) n = 1 Newtonian fluid; (2) n = 0.7; (3) n = 0.5; (4) n = 0.3.

viscosity profiles are given in Fig. 4 for fixed λ and varying n, and for fixed n and varying λ .

The velocity profiles are similar for the three fluid types, Fig. 2(a), 3(a) and 4(a). In overall, for increasing shear-thinning effects, i.e increasing B for Bingham model or decreasing n for power-law and Carreau models, the velocity gradient increases in absolute value at the internal wall and decreases at the external one. Concerning the viscosity profile, as can be expected, μ^b increases from the inner to the outer wall, where the shear rate is lower. If the inner wall shear viscosity is used as the reference, it can be observed that the overall viscosity increases with the shear-thinning effect. For Bingham and power-law fluids, the viscosity gradient $d\mu^b/dr$ at the inner wall increases with increas-

Fig. 5. Couette flow of a Carreau fluid for $\eta = 0.5$, n = 0.3 and different values of λ . (a) Basic azimuthal velocity profiles: (1) $\lambda = 0$ Newtonian fluid; (2) $\lambda = 1$; (3) $\lambda = 10$ and (--) power-law fluid. (b) Basic viscosity profiles: (1) $\lambda = 0$ Newtonian fluid; (2) $\lambda = 1$; (3) $\lambda = 10$; (4) $\lambda = 100$ and (--) power-law fluid.

ing B or decreasing n, Fig. 2(b) and 3(b). For Carreau fluid, Fig. 4(b) and 5(b), two behaviors are observed according to the value of λ . For $\lambda \leq O(1)$, the viscosity gradient is maximum at the inner wall, whereas for larger λ , the viscosity gradient is maximum at the outer wall. This is consistent with the fact that we can recover the power law model for large values of λ .

4 Linear stability equations

An infinitesimal perturbation $(\epsilon u', \epsilon p')$ is superimposed upon the basic flow.

$$\{\boldsymbol{U}, P, \boldsymbol{\tau}\} = \left\{\boldsymbol{U}^{\boldsymbol{b}}, P^{\boldsymbol{b}}, \boldsymbol{\tau}^{\boldsymbol{b}}\right\} + \varepsilon \left\{\boldsymbol{u'}, p', \boldsymbol{\tau'}\right\} . \tag{21}$$

The momentum equations are linearized around $\left(\boldsymbol{U}^{b},P^{b}\right)$ to yield

$$\nabla \cdot \boldsymbol{u}' = 0 \tag{22}$$

$$\frac{\partial \boldsymbol{u}'}{\partial t} + Re\left[\left(\boldsymbol{U}^{b}.\boldsymbol{\nabla}\right)\boldsymbol{u}' + \left(\boldsymbol{u}'.\boldsymbol{\nabla}\right)\boldsymbol{U}^{b}\right] = -\boldsymbol{\nabla}p' + \boldsymbol{\nabla}.\boldsymbol{\tau}'.$$
(23)

Using Taylor's expansion at the first order of the effective viscosity about the base flow, it can be shown that the perturbation of the shear-stress tensor is expressed as:

$$\boldsymbol{\tau}' = \frac{1}{\varepsilon} \left\{ \boldsymbol{\tau} \left(\boldsymbol{U}^b + \varepsilon \boldsymbol{u}' \right) - \boldsymbol{\tau} \left(\boldsymbol{U}^b \right) \right\} = \mu^b \dot{\boldsymbol{\gamma}} \left(\boldsymbol{u}' \right) + \left(\mu_t - \mu^b \right) \boldsymbol{A}$$
 (24)

where the tangential viscosity μ_t has been introduced:

$$\mu_t = \mu \left(\mathbf{U}^b \right) + \frac{\partial \mu}{\partial \dot{\gamma}_{r\theta}} \left(\mathbf{U}^b \right) \dot{\gamma}_{r\theta} \left(\mathbf{U}^b \right). \tag{25}$$

For Bingham and Power-law fluids, the explicit expressions of μ_t are given respectively by:

$$\mu_t = 1; \quad \text{and} \quad \frac{\mu_t}{\mu^b (r = R_1)} = n \left(\frac{R_1}{r}\right)^{\frac{2}{n}(n-1)}.$$
 (26)

The components of tensor \boldsymbol{A} are all zero except for $A_{1,2} = A_{2,1} = \dot{\gamma}_{r\theta}(\boldsymbol{u}')$. The anisotropy of the perturbation $\boldsymbol{\tau}'$ of the deviatoric stress tensor is a consequence of the nonlinear rheological behavior $\mu(\dot{\gamma})$ and the anisotropy of the base flow.

The solution is sought under the shape of normal modes

$$\{\boldsymbol{u}', p'\} = \{\boldsymbol{u}(r), p(r)\} \exp\left[\sigma t + i(m\theta + kz)\right], \tag{27}$$

 $u(r) = u(r) e_r + v(r) e_\theta + w(r) e_z$, $k \in \mathbb{R}$ is the axial wave number and $m \in \mathbb{Z}$ is the azimuthal wave number. The real part of the complex pulsation $\mathcal{R}e(\sigma)$ is the growth rate and the imaginary part allows to define the axial and angular phase velocities. Substituting the above solution ansatz into the linearized continuity and momentum equations (22,23) yields

$$0 = D_* u + \frac{imv}{r} + ikw,$$

$$\sigma u = -Re \frac{V^b}{r} (imu - 2v) - Dp + \mu^b \left[\Delta u - \frac{2imv}{r^2} - \frac{u}{r^2} \right]$$

$$+ 2 \left(D\mu^b \right) Du + \frac{im}{r} \left(\mu_t - \mu^b \right) \left(\tilde{D}v + \frac{im}{r} u \right),$$

$$\sigma v = -Re \left(uD_* V^b + \frac{V^b}{r} imv \right) - \frac{im}{r} p + \mu^b \left[\Delta v + \frac{2imu}{r^2} - \frac{v}{r^2} \right]$$

$$+ \left(D\mu^b \right) \left[Dv - \frac{v}{r} + \frac{imu}{r} \right] + D_* \left[\left(\mu_t - \mu^b \right) \left(\tilde{D}v + \frac{imu}{r} \right) \right]$$

$$+ \left(\mu_t - \mu^b \right) \left[\frac{1}{r} \left(\tilde{D}v + \frac{imu}{r} \right) \right],$$

$$\sigma w = -Re \frac{V^b}{r} imw - ikp + \mu^b \Delta w + \left(D\mu^b \right) \left[Dw + iku \right],$$

$$(31)$$

where
$$D = \frac{\mathrm{d}}{\mathrm{dr}}$$
, $D_* = D + \frac{1}{r}$, $\tilde{D} = D - \frac{1}{r}$ and $\Delta = D^2 + \frac{1}{r}D - \frac{m^2}{r^2} - k^2$.
The system of equation (28, 31) can be rewritten in terms of two components

of the velocity (u, v) for $k \neq 0$ or (v, w) for $m \neq 0$. The different formulations lead to a generalized eigenvalue problem which can be written formally as

$$\mathcal{L}\mathbf{q} = \sigma \mathcal{M} \,\mathbf{q},\tag{32}$$

where $\mathbf{q} = (u, v)^T$, $(u, w)^T$ depending on the formulation adopted. Operators \mathcal{L} and \mathcal{M} are given in the appendix. If $\mathcal{R}e(\sigma) < 0$ for all eigenvalues, the base flow is stable while if there exists a value of σ such as $\mathcal{R}e(\sigma) > 0$, the base flow becomes unstable. The condition $\mathcal{R}e(\sigma) = 0$ defines the critical threshold.

5 Numerical method

The eigenvalue problem is discretized by expanding the perturbation fields u and v (u and w) in a truncated series of orthogonal Chebyshev polynomials in $y = 2r - (1 + \eta)/(1 - \eta)$: $u = \sum_{n=0}^{N} a_n T_n(y)$ and $v = \sum_{n=0}^{N} b_n T_n(y)$. A collocation method where the equations are evaluated at the Gauss-Lobatto points is used. The eigenvalue problem is then transformed into its discrete form. Errors in the spectrum introduced by an insufficient resolution of the eigenvectors and which are characterized by a splitting of the spectrum [24], affect only the eigenvalues with large $|\mathcal{R}e(\sigma)|$. For instance, at $\eta = 0.5$, Re = 70 and N = 50, for all the fluids considered in the paper, the splitting is observed only for $\mathcal{R}e(\sigma) < -3000$, thus very far from the critical mode.

5.1 Convergence

To test the convergence of the numerical method, the computations of the critical conditions are made for different truncatures N. The result is illustrated in Tables 1 and 2 for Bingham and power-law fluids respectively. It is observed that thirty collocation points provide sufficient accuracy for the rheological parameters considered. The results given in the paper were obtained with N=40. Periodically, numerical tests were done to ensure convergence and accuracy.

N	10	20	30	40	50
Re_c	127.73265	127.74943	127.74943	127.74943	127.74943
k_c	3.183604	3.183699	3.183708	3.183707	3.183706

Table 1 Convergence tests for a Bingham fluid at $\eta = 0.5$ and B = 1.

N	10	20	30	40	50
Re_c	71.99404	72.35036	72.35046	72.35046	72.35046
k_c	3.885593	3.867630	3.867602	3.867669	3.867670

Table 2 Convergence tests for a power-law fluid at $\eta = 0.5$ and n = 0.3.

Fig. 6. Critical Reynolds number of a Newtonian fluid versus the radius ratio η . (o) Our results; (\square) Chandrasekhar's [25] result at $\eta = 0.5$ and k = 3.20; (--) Chandrasekhar's [25] result using a narrow gap approximation and k = 3.12.

5.2 Validation

As a first test of validation we have compared the critical Reynolds numbers for a Newtonian fluid at different radius ratios η , given by our program, to the ones of Chandrasekhar [25]. A very good agreement is found as can be seen in Fig. 6.

6 Computational results

The results section consists of three parts. The first one deals with the case of an axisymmetric disturbance (m = 0), the second one that of a homogeneous disturbance in the axial direction (k = 0) and the third one that of a three-dimensional disturbance.

6.1 Axisymmetric perturbation: m = 0

In the axisymmetric case, (u, v) formulation is used.

6.1.1 Eigenvalues' spectra

Eigenvalues spectra for Newtonian, power-law, Bingham and Carreau fluids at the critical conditions and for $\eta=0.5$ are shown in Fig. 7. The imaginary part of most of the eigenvalues is zero, particularly the least stable modes, i.e. the eigenmodes are not a traveling wave. One can note that the pairing of the eigenmodes observed for Newtonian fluids disappears progressively with increasing the shear-thinning behavior, this is particularly visible for power-law and Bingham fluids.

Fig. 7. Eigenvalues' spectra at the critical conditions for $\eta = 0.5$. (a) Newtonian fluid $Re_c = 68.75$ and $k_c = 3.12$. (b) Power-law fluid with n = 0.3, $Re_c = 72.4$ and $k_c = 3.9$. (c) Bingham fluid with B = 10, $Re_c = 950$ and $k_c = 9.4$. (d) Carreau fluid with $\lambda = 10$, n = 0.3, $Re_c = 14.1$ and $k_c = 3.69$.

6.1.2 Critical conditions

Case of power-law fluids

Figure 8(a) shows the variation of the critical Reynolds number as a function of the shear-thinning index n for different radius ratios η . Our results confirm those obtained by Jastrzebski *et al.*[11]. The influence of shear-thinning appears stabilizing or destabilizing depending on the radius ratio and the range of the shear-thinning index. If we use instead the inner wall shear viscosity

Fig. 8. Variation of the critical Reynolds number as function of shear-thinning index for a power-law fluid at different radius ratios. (o) Our results; (*) Jastrzebski *et al.*[11]. (a) The Reynolds number is defined with a nominal shear-rate viscosity $\hat{\mu}_{ref} = \hat{K} \left(\hat{R}_1 \hat{\Omega}_1 / \hat{d} \right)^{n-1}$. (b) The Reynolds number is defined with the inner wall shear-rate viscosity, Eq. (33).

 $\hat{\mu}^b(\hat{R}_1)$ in the definition of the Reynolds number

$$Re_{cw} = \frac{\hat{\rho}\hat{R}_1\hat{\Omega}_1\hat{d}}{\hat{\mu}^b(\hat{R}_1)},\tag{33}$$

with the conversion factor form from Re_c to Re_{cw} for Bingham and Power-law fluids given respectively by:

$$\frac{Re_c}{Re_{cw}} = 1 + \frac{B}{\tau_1^b} \quad \text{and} \quad \frac{Re_c}{Re_{cw}} = \left[\frac{2}{n} \frac{1}{R_1} \frac{1}{1 - \eta^{2/n}} \right]^{n-1},$$
(34)

it will be observed that the shear-thinning behavior delays the appearance of the Taylor vortices for all η as shown in Fig. 8(b). This effect increases with decreasing η . As expected, for η close to 1, the azimuthal velocity profile is practically linear and therefore the shear rate and the shear viscosity are practically constant in the annular space, leading to a critical Reynolds number Re_{cw} almost independent of n.

The influence of the shear-thinning index on the critical wave number and therefore on the size of the Taylor vortices is shown in Fig. 9. One can note that for a given shear-thinning index, the axial wavelength decreases with decreasing η . For instance, at $\eta = 0.4$ and n = 0.3, the axial wavelength is smaller than half that obtained in the case $\eta = 0.9$ and n = 0.3. This may be related to the stronger viscosity stratification between the inner and the outer cylinders as indicated by the curve (4) in Fig. 3(b).

The contours of iso-values of the radial velocity component for Newtonian

Fig. 9. (a) Variation of the critical axial wave number with the shear-thinning index, for power-law fluid at different radius ratio. (b) Dimensionless size of the Taylor vortices as function of the shear-thinning index.

Fig. 10. Equally spaced contours of the radial component u of the velocity perturbation for a radius ratio $\eta=0.4$. Continuous and dotted lines correspond to positive and negative values of u. (a) Newtonian fluid at $Re=Re_c=68.2$ and $k=k_c=3.18$. (b) Power-law fluid with n=0.3 at $Re_w=Re_{cw}=405.1$ and $k=k_c=5.25$.

and power law fluids, represented in Fig. 10, illustrate clearly the influence of the shear-thinning behavior. For n=0.3, the contours are strongly squeezed against the inner wall, where the viscosity is lower. This behavior is also illustrated by the contours of azimuthal vorticity,

$$\omega_{\theta} = \frac{\partial w}{\partial r} - \frac{\partial u}{\partial z},\tag{35}$$

which are displayed in the Fig. 11. Each vortex is bounded by radial inflow and outflow jets. Over one axial wavelength, the vortices alternate in sign. Regions of opposite sign vorticity exist outside each vortex. These regions do not represent separate vortices but results from changing sign of $\partial w/\partial r$. These regions are clearly represented for Newtonian fluid. For power-law fluid, the region of opposite sign vorticity is very thin near the inner wall, and not represented near the outer wall, because $\partial w/\partial r$ is too weak.

Fig. 11. Contours of azimuthal vorticity ω_{θ} at the critical conditions for $\eta = 0.4$. Continuous and dotted lines correspond to positive and negative values of ω_{θ} . (a) Newtonian fluid. (b) power-law fluid with n = 0.3.

Case of Bingham fluid

The variation of the critical Reynolds number with the Bingham number is shown in Fig. 12(a). Once again, we note an increase of Re_{cw} with increasing the viscosity stratification induced by the Bingham number ($\mu = 1 + B/\dot{\gamma}$). Our results represented by dashed and dashed-dotted lines for $\eta = 0.5$ and $\eta = 0.883$ respectively, confirm those given by Landry et al. [19]. The axial size of the Taylor vortices is estimated from the critical wave number scaled with the width of the yielded zone, $k_c = k_c \times (R_0 - R_1)$, and is represented in Fig. 12(b) as a function of the Bingham number. The vertical dotted line at B_{ℓ} separates the domain of B where the annular space is completely yielded from that where a plug zone is attached to the outer cylinder. Below the limit value, B_{ℓ} the variation is in agreement with that observed for power law fluids. For large Bingham number, $B > B_{\ell}$, we also recover the behavior observed in Fig. 9(a) at η close to 1. The present results are qualitatively compatible with those obtained by Graebel [17] for $\eta \to 1$. Figure 13 shows the contours of the radial velocity and azimuthal vorticity for a large value of B. The viscosity is almost constant in the very narrow yielded zone. Close to the yield surface, μ increases strongly and tends to infinite.

Case of Carreau fluid

As mentioned in the introduction, the data dealing with the critical conditions for Carreau fluids are very limited. The results given by Coronado et~al.~[16] are reported in Fig. 14. They were computed for $\lambda=0.1$, i.e, low shear-thinning effect, and an aspect ratio defined by the gap length \hat{L} to the width gap \hat{d} ratio, $\hat{L}/\hat{d}=10$. For η close to 1, significant differences are observed with our results which are practically independent of n due to the weak value of λ . The discrepancies between our results and those given by Coronado et~al.~[16] are expectable. Indeed, the computation domain considered by Coronado et~al.~[16] is enclosed by endwalls that confine the fluid in the axial direction. This confinement destroys the translation invariance and results in a basic

Fig. 12. (a) Critical Reynolds number versus Bingham number for two radius ratios: $\eta = 0.5$: (o) Landry *et al.* [19], (\diamond) Caton [1], (\triangle) Lockett *et al.* [12], (--) our results; $\eta = 0.883$ (\square) Landry *et al.* [19], (-.-) our results. (b) Scaled critical wave number versus Bingham number for two radius ratios ($-\circ-$) $\eta = 0.5$ and ($-\square-$) $\eta = 0.883$.

Fig. 13. Bingham fluid with B=100 at the critical conditions $Re_{cw}=2112, k_c\times(R_0-R_1)=2.52$. The radius ratio is $\eta=0.5$. (a) Equally spaced contours of the radial component u of the velocity perturbation. (b) Contours of azimuthal vorticity ω_{θ} .

flow which is not purely azimuthal as in our case, but also has axial and radial components. The discontinuity of the velocity at the endwalls generates small vortices adjacent to the endwalls which may propagate towards the center of the domain, therefore modifying the critical conditions comparatively to purely azimuthal base flow.

Li and Khayat [15] also calculated the critical Reynolds number for low shear-thinning fluid. Using Taylor expansion around $\lambda^2\dot{\gamma}^2$ considered as a small parameter, the viscosity is written as: $\mu=1+\alpha^2\dot{\gamma}^2$, with $\alpha=(1-\mu_\infty/\mu_0)(n-1)/2\lambda^2$. We have not reported their results in Fig. 14 or 15, because the values of α considered by the authors lead to negative values of n, if $\mu_\infty/\mu_0=0$ and λ is weak. We have not reported either the results of Ashrafi and Khayat [14], because unlike here, they considered the unrealistic free (slip) boundary conditions.

Our results are displayed in Fig. 15(a) for a wide range of λ and different

Fig. 14. Critical Reynolds number as a function of the radius ratio η for a Carreau fluid at $\lambda=0.1$ and different values of n. (--) Newtonian fluid, (\bullet) Coronado et al. [16] for n=0.9; (\blacksquare) Coronado et al. [16] for n=0.8; (\blacktriangle) Coronado et al. [16] for n=0.6. For $\eta<0.8$, the critical values of Re are very close for the three sets of the rheological parameters considered. Our results (\Box) are almost independent on n for the whole η range.

Fig. 15. (a) Critical wall Reynolds number and (b) wave number for a Carreau fluid with $\eta=0.5$ as a function of the dimensionless constant time λ for different values of the shear-thinning index: (o) n=0.7, (\square) n=0.5 and (\triangle) n=0.3. (--) Power-law fluid.

values of n. The increase of stability of the Couette flow with increasing the shear-thinning behavior is clearly shown. From $\lambda = 0$, the critical Reynolds number increases and then tends asymptotically towards the value obtained for power-law fluids. The evolution of the critical wave number with the the dimensionless constant time λ for different shear-thinning index is described by Fig. 15(b). We note that the asymptotic values of k_c at large λ are different from those obtained for a power law fluid (see Fig. 9a)

6.1.3 Energy equation

If the viscosity perturbation is not taken into account, the critical Reynolds numbers are found to be higher as it is shown by Fig. 16. This can be interpreted by considering the energy equation, obtained using the scalar product Fig. 16. Critical conditions for a power-law fluid at $\eta = 0.5$ as a function of the shear-thinning index n. (1) the viscosity perturbation is taken into account, $\mu_t - \mu^b \neq 0$; (2) the viscosity perturbation is excluded artificially, $\mu_t - \mu^b = 0$. (a) Critical wall Reynolds number. (b) Critical wave number.

of the linearized momentum equation with the complex conjugate u^* and by integrating between the two cylinders

$$\mathcal{R}e(\sigma)||\mathbf{u}||^{2} = -Re \int_{R_{1}}^{R_{2}} \dot{\gamma}_{r\theta}^{b} \frac{u^{*}v + uv^{*}}{2} dr
- \int_{R_{1}}^{R_{2}} \mu^{b} \left[\frac{1}{2} \left(|\dot{\gamma}_{rr}^{\prime}|^{2} + |\dot{\gamma}_{\theta\theta}^{\prime}|^{2} + |\dot{\gamma}_{zz}^{\prime}|^{2} \right) + |\dot{\gamma}_{r\theta}^{\prime}|^{2} + |\dot{\gamma}_{rz}^{\prime}|^{2} + |\dot{\gamma}_{\theta z}^{\prime}|^{2} \right] dr
+ \int_{R_{1}}^{R_{2}} \left(\mu^{b} - \mu_{t} \right) |\dot{\gamma}_{r\theta}^{\prime}|^{2} dr,$$
(36)

where
$$\dot{\gamma}_{ij} = \dot{\gamma}_{ij}(\boldsymbol{u})$$
, $||\boldsymbol{u}||^2 = \int_{R_1}^{R_2} (|u|^2 + |v|^2 + |w|^2) r dr$ and $|u|^2 = uu^*$.

The third term of the right-hand-side originates in the viscosity perturbation. It is positive definite and produces a reduction of viscous dissipation and thus a decrease of the critical Reynolds number. A phenomenological interpretation can also be made: when an infinitely small perturbation is imposed to the flow, the stress $\tau_{r\theta}$ is modified of $\delta\tau_{r\theta}$ and the shear rate $\dot{\gamma}$ of $\delta\dot{\gamma}_{r\theta}$, so that the perturbation only sees the tangential viscosity $\mu_t = \delta\tau_{r\theta}/\delta\dot{\gamma}_{r\theta}$ and not the effective viscosity.

The energy equation (36) can be written in symbolic form as

$$\mathcal{R}e(\sigma)\mathcal{I}_1 = Re\,\mathcal{I}_2 - \mathcal{I}_3 \tag{37}$$

where $Re \mathcal{I}_2$ is a production term which corresponds to a transfer of energy from the base flow to the perturbation, and \mathcal{I}_3 is a dissipation term associated to viscous effects. Following Govindarajan *et al.* [26], it is convenient to compute and compare the space-averaged production and dissipation terms Γ_{\pm} defined by

Fig. 17. Disturbance kinetic energy terms for a Newtonian fluid at criticality, $Re_w = 68.316$ and k = 3.12. The production term $Re\mathcal{I}_2$ is plotted with a solid line and the dissipation term \mathcal{I}_3 is plotted with a dashed line. The space-averaged production and dissipation terms are equal since the conditions are critical, $\Gamma_+ = \Gamma_- = 28.073$.

$$\Gamma_{+} = Re \frac{\int_{R_{1}}^{R_{2}} \mathcal{I}_{2} dr}{\int_{R_{1}}^{R_{2}} \mathcal{I}_{1} dr}, \qquad \Gamma_{-} = \frac{\int_{R_{1}}^{R_{2}} \mathcal{I}_{3} dr}{\int_{R_{1}}^{R_{2}} \mathcal{I}_{1} dr}$$
(38)

At criticality, the transfer of energy from the base flow to the disturbance motion is exactly balanced by viscous dissipation, $\Gamma_+ = \Gamma_-$, as shown in Fig. 17 for the case of a Newtonian fluid. The effect of viscosity stratification on the energy budget can be appreciated by comparing the results obtained for a Newtonian fluid (Fig. 17) with those given in Fig. 18 for a power law fluid. In the latter case we have $Re_w = 68.316$, k corresponds to the critical wave number value for n = 0.5 or 0.3. With increasing shear thinning behavior, we observe that the average viscous dissipation remains close to that in Newtonian fluid while the production term is strongly reduced, rendering the flow more stable compared to the Newtonian case. This is clearly illustrated by Fig. 19. Hence, The main factor determining stability or instability of the flow is the exchange of energy between the base flow and the disturbance, which is driven by the phase change between the two fluctuating velocity components, caused by the viscosity stratification.

6.1.4 Discussion

In this section, we discuss the relevance of the different expressions of the reference viscosity used in the literature as well as the radial position where the viscosity gradient has the largest effect on the flow stability.

Reference viscosity

The relevance of the reference viscosity $\hat{\mu}_{ref}$ proposed in the literature can be

Fig. 18. Effect of the viscosity stratification on the energy budget for a power-law fluid, $Re_w = 68.316$ and $\eta = 0.4$. (Continuous line) Energy production $Re\mathcal{I}_2$ and (dashed line) energy dissipation \mathcal{I}_3 . (a) $n=0.7, k=3.20, \Gamma_+=15.436$ and $\Gamma_{-} = 23.450$. (b) n = 0.3, k = 5.25, $\Gamma_{+} = 1.456$ and $\Gamma_{-} = 27.232$.

Fig. 19. Space averaged (\blacktriangle) production Γ_+ and (\bullet) dissipation Γ_- terms for a power-law fluid with $\eta = 0.4$ as a function of shear-thinning index n.

- assessed by plotting the radial position r_b where $\hat{\mu}^b(r_b) = \hat{\mu}_{ref}$.

 For power-law fluid with n=0.4 and for a radius ratio $\eta=0.4$, the radial position r_b where $\hat{\mu}(r_b) = \hat{K} \left(\hat{R}_1 \hat{\Omega}_1 / \hat{d} \right)^{n-1}$ is represented in Fig. 20 by a dotted line. We have also represented $Re\mathcal{I}_2$ and \mathcal{I}_3 at criticality. The viscous dissipation takes place mainly at the inner wall and the exchange of energy is also localized near that wall. The reference viscosity $\hat{K} \left(\hat{R}_1 \hat{\Omega}_1 / \hat{d} \right)^{n-1}$ is attained further in the gap, i.e. that is outside the region of interest.
- For Carreau fluid, $\dot{\gamma}_{r\theta}^b$ is never zero in the annular gap, therefore it is counterintuitive to use the zero-shear-rate viscosity $\hat{\mu}_0$ as a reference viscosity.
- For Bingham fluid, using the plastic viscosity $\hat{\mu}_p$ as a reference viscosity is not appropriate since $\hat{\mu}_b = \hat{\mu}_p$ only if $\dot{\gamma}_{r\theta}^b \to \infty$.

For all the three fluids considered, the reference viscosity is either outside the region of interest or does not match the base viscosity at any point of the annular gap. Since the viscous dissipation and exchange of energy between the base flow and the disturbance takes place mainly at the inner wall, it seems more appropriate to use the viscosity at that wall as the reference viscosity. This choice is supported by the second part of this section, where it is shown that indeed, the region of interest is localized near the inner wall.

Position of viscosity gradient leading to largest effect on flow stability

It is interesting to note that the viscosity profiles Fig. 5(b) obtained for Carreau fluids with n=0.3 and $\lambda \geq 10$ lead to very close values of Re_c (Fig. 15a). The analysis of the curves (3) and (4) in Fig. 5(b) indicates that the viscosity gradient near the inner cylinder has a significant effect on the flow stability while a viscosity gradient far from the inner wall has practically no effect on the flow stability. To clarify this idea, we have used the approach proposed by Govindarajan et al. [27,26] for plane Poiseuille flow that we have adapted to the case of circular Couette flow. We consider the Couette-Taylor flow of two fluids of viscosities $\hat{\mu}_1$ and $\hat{\mu}_2 > \hat{\mu}_1$, Fig. 21(a). The least viscous fluid is located near the inner rotating wall, $R_1 < r < h$, and the most viscous near the outer wall, $h + e < r < R_2$. Viscosity evolves continuously at the interface between the two fluids over a mixing layer, h < r < h + e, leading to the viscosity profile $\mu(r) = \hat{\mu}(r)/\hat{\mu}_1$,

$$\mu = 1 \text{ if } R_1 < r < h$$

$$\mu(r) = 1 + (\delta - 1)\xi^3 \left[10 - 15\xi + 6\xi^2 \right] \text{ if } 0 \le \xi \le 1 , \quad \xi = (r - h)/e \quad (39)$$

$$\mu = \delta \text{ if } h + e < r < R_2$$

that is plotted in Fig. 21(b). The expression of viscosity in the mixing layer has been chosen as in Govindarajan et al. [27], so that the viscosity and its two first derivatives are continuous in the whole gap. The base state is then computed with a classical shooting method associated to a Newton Raphson method. A stability analysis, in which the diffusion of one fluid into another is neglected, is then conducted and the critical Reynolds number for instability perturbation equations are obtained showing viscosity stratification. Even if this approach leaves the viscosity profile unchanged when perturbating the flow, unlike the shear-thinning models considered before, it remains relevant to highlight clearly the viscosity stratification effect. The critical value of the

Reynolds number defined as $Re = \frac{\hat{\rho}\hat{R}_1\hat{\Omega}_1\hat{d}}{\hat{\mu}_1}$ is computed for several mixing layer locations h + e/2, widths e and viscosity contrast δ . The results in Fig. 22 for a mixing layer of thickness e = 0.1 centered at r = h + e/2 = 0.55, and a viscosity ratio of $\delta = 1.1$ show that the existence of a viscosity gradient is a source of stabilization and that the closer the mixing layer to the inner wall, the higher the stabilization, with a maximum at a distance close to the wall. Some more simulations showed that for increasing m, the stabilization increases even more near the wall. We may extrapolate from this simple study, without diffusion at the fluids interface, that it is the region near the inner wall that dominates the stability of the Couette-Taylor flow of a shear-thinning

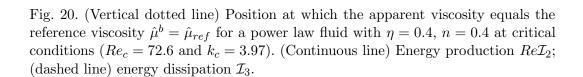


Fig. 21. (a) Scheme of the mixing layer joining two fluids of different viscosities. (b) Viscosity profile for a radius ratio $\eta = \hat{R}_2/\hat{R}_1 = 0.4$, a mixing layer of thickness e = 0.1 and centered at r = h + e/2 = 0.55, and a viscosity contrast $\delta = \mu_2/\mu_1 = 1.1$.

fluid.

6.2 Homogeneous perturbation in the axial direction

By setting k = 0, the linear stability equations given by the (u, w) formulation in Appendix A.2 reduce to two decoupled differential equations: (i) a fourth-order differential equation for u and (ii) a second order differential equation for w:

Fig. 22. Critical Reynolds number as a function of the location of the mixing layer, centered at r = h + e/2, for a radius ratio $\eta = 0.4$, a layer thickness of e = 0.1 and a viscosity ratio $\delta = 1.1$. The dashed line indicates the critical value of Re for a Newtonian fluid.

$$\sigma \left[D_*^2 u + \frac{1}{r} D_* u - \frac{m^2}{r^2} u \right] = Re \frac{i \, m}{r} \left[u \, D D_* V_b - V_b \left(D_*^2 u + \frac{2}{r} D_* u - \frac{m^2}{r^2} u \right) \right]$$

$$+ \mu^b \left[D_*^2 + \frac{1}{r} D_* - \frac{m^2}{r^2} \right]^2 u - 4 \frac{m^2}{r^2} D \mu^b D_* u + \left[D_*^2 + \frac{3}{r} D_* + \frac{m^2}{r^2} \right] \left[\left(\mu_t - \mu^b \right) \left(D_*^2 u - \frac{1}{r} D_* u - \frac{m^2}{r^2} u \right) \right], (40)$$

$$\sigma w = -Re \frac{i \, m}{r} V_b \, w + \mu^b \left[\frac{1}{r} D \left(r \, D w \right) - \frac{m^2}{r^2} w \right] + D \mu^b \, D w.$$

$$(41)$$

We first consider the set of eigenmodes of (41). Using a variational formulation, i.e., multiplying by the complex conjugate w^* and integrating between the outer and the inner cylinders, it can be shown that

$$\mathcal{I}m(\sigma) \int_{R_1}^{R_2} |w|^2 dr = -Re \, m \int_{R_1}^{R_2} \frac{V^b}{r} |w|^2 dr, \tag{42}$$

and

$$\Re(\sigma) \int_{R_1}^{R_2} |w|^2 dr = -\int_{R_1}^{R_2} \mu^b \left(|Dw|^2 + \frac{m^2}{r^2} |w|^2 \right) dr.$$
 (43)

It is clear that the eigenmodes of (41) are always damped, $\Re(\sigma) < 0$. Concerning the eigenmodes of Eq. (40), the corresponding eigenvalues' spectra are displayed in Fig. 23, for Newtonian and shear-thinning fluids at two wall Reynolds numbers: $Re_w = 100$ and 500. The eigenmodes associated with the vertical branch have an angular phase velocity which decreases with increasing the shear-thinning effects. Unlike Caton (2006) [1], for all the range of the rheological parameters considered in the paper, $0.1 \le n \le 1$ and $0 \le B \le 500$, we have not found any instability. This was confirmed by computations performed

Fig. 23. Eigenvalues spectra at $\eta = 0.5$, k = 0, m = 1 and two Reynolds numbers (\circ) $Re_w = 100$ and (\square) $Re_w = 500$. (a) Newtonian fluid. (b) Power-law fluid with n = 0.3.

by anonymous referee. Actually, Caton [1] found that with increasing shear-thinning effects, the shape of the critical mode changes sharply from toroidal axisymmetric vortices to longitudinal vortices. This would mean a change in the instability mechanism. We believe that at the linear level in the perturbation equations, the shear-thinning does not alter the instability mechanisms. The only effect of shear-thinning is to shift the critical conditions as indicated in the existing literature, although for other geometrical configurations, (see for instance [26–28]). As Newtonian Couette flow between two coaxial cylinders, where the outer cylinder is fixed and the inner is rotating, is linearly stable with respect to a homogeneous perturbation [29] in the axial direction, it is therefore not surprising to find a similar result for a shear-thinning fluid.

6.3 Three-dimensional case

In the 3D situation, (u,v) formulation is used to compute the critical conditions. Figure 24 shows marginal stability curves for different azimuthal wave numbers m. It is clearly observed that Re_c increases with increasing the azimuthal wave number. The minimum is always achieved for the axisymmetric case, even for highly shear-thinning fluids (n = 0.1) or (B = 50). This is in contradiction with the results of Caton [1]. The shape of the marginal stability curves at low axial wave numbers confirms that the Couette flow is linearly stable at k = 0.

Fig. 24. Marginal stability curves at $\eta=0.5$ and different values of the azimuthal wave numbers. (a) Bingham fluid with B=50. (b) Power-law fluid with n=0.1

Remark

n 3D situation, even for a newtonian fluid, our results confirmed by anonymous referee are in disagreement with those given by Caton[1].

7 Conclusion

Three-dimensional linear stability analysis of the circular Couette flow of a shear-thinning fluid with and without yield stress was investigated in this paper. This study was motivated by some surprising results as well as discrepancies in the results given in the literature. Part of these discrepancies is due to the scaling of the viscosity which is addressed here. Three types of rheological models were considered: power-law, Carreau and Bingham models. Looking for normal mode solutions, the linearized perturbation equations lead to an eigenvalue problem solved using pseudo-spectral collocation method. An axisymmetric perturbation was first assumed and the critical Reynolds number was computed for different shear-thinning strengths, n or B, and for different radius ratios η . The critical conditions were successfully compared to several previous results of the literature. In all cases, it is observed that when the viscosity is scaled with the inner wall shear-viscosity, shear-thinning has a stabilizing effect, i.e. the appearance of the Taylor-vortices is delayed. Analysis of the disturbance energy equation allows to show that this stabilizing effect is due to the reduction of the energy exchange between the base flow and the disturbance. Complementary study was carried out to highlight that the viscosity gradient localized near the inner cylinder has the largest stabilizing effect while a viscosity gradient far for the inner wall has practically no effect. The wavelength k_c of the most unstable mode was shown to depend on both n or B and η , especially for large gaps (low η) for which Taylor vortices are squeezed against the inner wall where the viscosity is lower. For a Bingham fluid, the dependence of k_c to the Bingham number B changes when a nonyielded zone appears close to the outer cylinder.

Three dimensional perturbations were then investigated but it was found that the most unstable modes are axisymmetric, even for very strong shear-thinning fluids. This result is in contradiction to the work of Caton (2006) who predicted the appearance of vertical cells for low n or high B.

Acknowledgements

This research was supported by PHC (Partenariat Hubert Curien) under grant 07 MDU 717. The authors thank an anonymous referee for his efforts to confirm our results.

A Operators involved in the linearized perturbation equations:

 $A.1 \quad (u,v) \ formulation$

The eigenvalue problem reads

$$\mathcal{L}\mathbf{q} = \sigma \mathcal{M} \mathbf{q} , \qquad (A.1)$$

where $\mathbf{q} = (u, v)^T$ and operators \mathcal{M} and \mathcal{L} are expressed below

$$\mathcal{M} = \begin{pmatrix} \mathcal{S} & \frac{i\,m}{r}\,\tilde{D} \\ -\frac{i\,m}{k^2\,r}\,D_* & 1 + \frac{m^2}{k^2\,r^2} \end{pmatrix}$$

$$\mathcal{L} = \mathcal{L}_I + \mathcal{L}_{V1} + \mathcal{L}_{V2} + \mathcal{L}_{V3}$$

$$\mathcal{L}_{I} = Re \begin{pmatrix} \frac{i\,m}{r} \left[-\left(V^{b}\,\widetilde{D} + D\,V^{b} \right)\,D_{*} + k^{2}\,V^{b} \right] & -2\,\frac{k^{2}\,V^{b}}{r} + \frac{m^{2}}{r^{2}} \left(-\frac{2\,V^{b}}{r} + D\,V^{b} + V^{b}\,D \right) \\ -D_{*}\,V^{b} - \frac{m^{2}}{k^{2}\,r^{2}}\,V^{b}\,D_{*} & -\frac{i\,m}{r} \left(1 + \frac{m^{2}}{k^{2}\,r^{2}} \right)V^{b} \end{pmatrix}$$

$$\mathcal{L}_{V1} = \mu^{b} \begin{pmatrix} S^{2} & i \, m \left[\frac{2 \, k^{2}}{r^{2}} + D \, \Delta \frac{1}{r} \left(\Delta - \frac{2D}{r} + \frac{1}{r^{2}} \right) \right] \\ \frac{i \, m}{r} \left(-\frac{\Delta D_{*}}{k^{2}} + \frac{2}{r} \right) & S + \frac{m^{2}}{k^{2} \, r^{2}} \left(\Delta - \frac{2D}{r} + \frac{1}{r^{2}} - k^{2} \right) \end{pmatrix}$$

$$\mathcal{L}_{V2} = D \mu^{b} \begin{pmatrix} D^{2} \, D_{*} + \Delta D_{*} - k^{2} \, D & \frac{i \, m}{r} \left(\Delta + D^{2} - \frac{4D}{r} + \frac{3}{r^{2}} \right) \\ -\frac{i \, m}{k^{2} \, r} \, D \, D_{*} & \left(1 + \frac{m^{2}}{k^{2} \, r^{2}} \right) \widetilde{D} \end{pmatrix}$$

$$+ D^{2} \mu^{b} \begin{pmatrix} k^{2} + D \, D_{*} & \frac{i \, m}{r} \, \widetilde{D} \\ 0 & 0 \end{pmatrix}$$

$$\mathcal{L}_{V3} = \left(\mu_t - \mu^b\right) \begin{pmatrix} \frac{k^2 \, m^2}{r^2} & -\frac{i \, k^2 \, m \, \widetilde{D}}{r} \\ \frac{i \, m \, D_*}{r} & \left(D + \frac{2}{r}\right) \, \widetilde{D} \end{pmatrix} + D \, \left(\mu_t - \mu^b\right) \begin{pmatrix} 0 & 0 \\ \frac{i \, m}{r} & \widetilde{D} \end{pmatrix}.$$

A.2 (u, w) formulation

The eigenvalue problem reads

$$\mathcal{L}\mathbf{q} = \sigma \mathcal{M} \mathbf{q} , \qquad (A.2)$$

where $\mathbf{q} = (u, w)^T$ and operators \mathcal{M} and \mathcal{L} are expressed below

$$\mathcal{M} = \begin{pmatrix} D_*^2 + \frac{1}{r}D_* - \frac{m^2}{r^2} & i k D + \frac{2 i k}{r} \\ k D_* & i k^2 + \frac{i m^2}{r^2} \end{pmatrix}$$

$$\mathcal{L} = \mathcal{L}_I + \mathcal{L}_{V1} + \mathcal{L}_{V2} + \mathcal{L}_{V3}$$

$$\mathcal{L}_{I} = Re \begin{pmatrix} \frac{i\,m}{r^{2}} \left(2\,D\,V^{b} + V^{b}\,D - 3\,V^{b}\,D_{*} + \frac{m^{2}\,V^{b}}{r} \right) & \frac{3\,k\,m\,V^{b}}{r^{2}} \\ \frac{i\,k\,m}{r} \left(D\,V^{b} - V^{b}\,D \right) & \frac{m}{r} \left(\frac{m^{2}\,V^{b}}{r^{2}} + k^{2}\,V^{b} \right) \end{pmatrix} \\ + Re \begin{pmatrix} \frac{i\,m}{r} \left[-\frac{DV^{b}}{r^{2}} + D^{2}V^{b} - V^{b}DD_{*} \right] & \frac{k\,m}{r} \left(V^{b}\,D + DV^{b} \right) \\ 0 & 0 & 0 \end{pmatrix} \\ \mathcal{L}_{V1} = \mu^{b} \begin{pmatrix} -\frac{2\,m^{2}}{r^{4}} & i\,k \left[\left(\frac{2}{r} + D \right) \left(D_{*}D - k^{2} \right) + \frac{2D_{*}D}{r} - \left(\frac{4}{r} + D \right) \frac{m^{2}}{r^{2}} \right] \\ k \left(\Delta + \frac{2D}{r} \right) D_{*} & i\,k^{2} \left(\Delta + \frac{2D}{r} \right) \\ + \mu^{b} \left(\frac{(\frac{2}{r} + D)}{r} \Delta D_{*} + \frac{2}{r} \left(D^{2} + \frac{D}{r} \right) D_{*} - \frac{m^{2}}{r^{2}} \Delta - \frac{m^{2}}{r^{4}} & 0 \\ \frac{2\,k\,m^{2}}{r^{3}} & 0 \end{pmatrix} \\ \mathcal{L}_{V2} = D\mu^{b} \begin{pmatrix} \frac{2}{r}\,D\,D_{*} - \frac{m^{2}}{r^{2}} \left(D - \frac{2}{r} \right) & i\,k \left[\Delta + \left(\frac{4}{r} + D \right) \,D \right] \\ k\,D\,D_{*} & i \left(k^{2} + \frac{m^{2}}{r^{2}} \right) D \end{pmatrix} \\ + D\mu^{b} \begin{pmatrix} \left[\left(D + \frac{2}{r} \right) \,D + \Delta \right] \,D_{*} & 0 \\ 0 & 0 \end{pmatrix} \\ + D^{2}\mu^{b} \begin{pmatrix} D\,D_{*} + \frac{m^{2}}{r^{2}} & i\,k\,D \\ 0 & 0 \end{pmatrix} \\ \mathcal{L}_{V3} = \left(\mu_{t} - \mu^{b} \right) \begin{pmatrix} \left[\left(\frac{5}{r} + D \right) \,D + \frac{3}{r^{2}} + \frac{2\,m^{2}}{r^{2}} \right] D\,D_{*} + \frac{m^{4}}{r^{4}} & i\,k \left[\frac{m^{2}}{r^{2}} + \frac{3}{r^{2}} + \left(\frac{5}{r} + D \right) \,D \right] D \\ k \left[\left(\frac{3}{r} + D \right) \,D + \frac{m^{2}}{r^{2}} \right] D_{*} & i\,k^{2} \left(D + \frac{3}{r} \right) D \end{pmatrix} \\ + D \left(\mu_{t} - \mu^{b} \right) \begin{pmatrix} \left(\frac{5}{r} + 2\,D \right) D\,D_{*} + \frac{m^{2}}{r^{2}} & i\,k\,D \\ 0 & 0 \end{pmatrix} \\ 0 & 0 \end{pmatrix}. \\ \end{pmatrix}$$

References

- [1] F. Caton. Linear stability of circular Couette flow of inelastic viscoplastic fluids. J. Non-Newtonian Fluid Mech., 134:148–154, 2006.
- [2] G.I. Taylor. Stability of viscous liquid contained between two rotating cylinders. *Phil. Trans. R. Soc. London.*, A223:289–343, 1923.
- [3] R. C. Di Prima and H. L. Swinney. Instabilities and transition in flow between concentric rotating cylinders. In *Hydrodynamic instabilities and the transition*

- to turbulence, pages 139–180. Springer Verlag, 1981.
- [4] H. Giesekus. Zur stabilitt von strmungen viskoelastischer flssigkeiten 1. ebene und kreisfrmige couette-strmung. *Rheol. Acta*, 5:239–252, 1966.
- [5] S. J. Muller, R.G. Larson, and E. S. G. Shaqfeh. A purely elastic transition in Taylor-Couette flow*. *Rheol. Acta.*, 28:499–503, 1989.
- [6] S. J. Muller R. G. Larson and E. S. Shaqfeh. A purely elastic instability in Taylor-Couette flow. J. Fluid. Mech., 218:573–600, 1990.
- [7] E. S. G. Shaqfeh, S. J. Muller, and R. G. Larson. The effects of gap width and dilute solution properties on the viscoelastic Taylor-Couette instability. *J. Fluid. Mech.*, 235:285–317, 1992.
- [8] A. Groisman and V. Steinberg. Mechanism of elastic instability in couette flow of polymer solutions: Experiments. *Phys. Fluids*, 10:2451–2463, 1998.
- [9] D. G. Thomas, B. Khomami, and R. Sureshkumar. Nonlinare dynamics of viscoelastic Taylor-Couette flow: effect of elasticity on pattern selection, molecular and conformation drag. J. Fluid. Mech., 620:353–382, 2009.
- [10] V. Sinevic, R. Kuboi, and A. W. Nienow. Power numbers, Taylor numbers and Taylor vortices in viscous Newtonian and non-Newtonian fluids. *Chemical Engineering Science*, 41:2915–2923, 1986.
- [11] M. Jastrzebski, H. A. Zaidani, and S. Wronski. Stability of Couette flow of liquids with power law viscosity. *Rheol. Acta.*, 31:264–273, 1992.
- [12] T. J. Lockett, S. M. Richardson, and W. J. Worraker. The stability of inelastic non-newtonian fluids in Couette flow between concentric cylinders: a finite-element study. *J. Non-Newtonian Fluid Mech.*, 43:165–177, 1992.
- [13] M.P. Escudier, I.W. Gouldson, and D.M. Jones. Taylor vortices in Newtonian and shear-thinning liquids. *Proceedings - Royal Society of London*, A 449 (1935):155–176, 1995.
- [14] N. Ashrafi and R. E. Khayat. Shear-induced chaos in Taylor-Vortex flow. *Phys. Rev. E*, 61:1455, 2000.
- [15] Z. Li and R.E. Khayat. A non-linear dynamical system approach to finite amplitude taylor-vortex flow of shear-thinning fluids. *International Journal for Numerical Methods in Fluids*, 45 (3):321, 2004.
- [16] O. Coronado-Malutti, P. R. Souza Mendes, and M. S. Carvalho. Instability of inelastic shear-thining liquids in a Couette flow between concentric cylinders. *Journal of Fluids Engineering*, 126:385–390, 2004.
- [17] W.P. Graebel. The hydrodynamic stability of a Bingham fluid in Couette flow. Proceedings of International Symposium on 2nd Order Effects in Elasticity, Plasticity and Fluid Dynamics, Haifa, Israel, April 2327, (ed. M. Reiner & D. Abir). Jerusalem Academic Press., pages 636–649, 1964.

- [18] J. Peng and K.Q. Zhu. Linear stability of Bingham fluids in spiral Couette flow. J. Fluid Mech., 512:21–45, 2004.
- [19] M.P. Landry, I.A. Frigaard, and D.M. Martinez. Stability and instability of Taylor Couette flows of a bingham fluid. *J. Fluid. Mech.*, 560:321–353, 2006.
- [20] C. D. Andereck, S. S. Liu, and H. L. Swinney. Flow regimes in a circular couette system with independently rotating cylinders. *J. Fluid Mech*, 164:155–183, 1986.
- [21] Z. H. Wan, J. Z. Lin, and Z. J. You. Non-axisymmetric instability in the Taylor-Couette flow of fiber suspension. *Journal of Zhejiang University SCIENCE*., 2005 6A:1–7, 2005.
- [22] R. Bird, R. Amstrong, and O. Hassager. Dynamics of polymeric liquids. Wiley Interscience, New York, 1987.
- [23] R. Tanner. Engineering rheology. Oxford University Press, New York, 2000.
- [24] P. J. Schmid and D. S. Henningson. Stability and transition in shear flows. Springer - Verlag, 2001.
- [25] S. Chandrasekhar. Hydrodynamic and hydromagnetic stability. Dover Publications, 1981.
- [26] R. Govindarajan, V. S. L'Vov, I. Procaccia, and A. Sameen. Stabilization of hydrodynamic flows by small viscosity variations. *Phys. Rev. E*, 2003:026310.1– 026310.11, 2003.
- [27] R. Govindarajan, V. S. L'vov, and I. Proccaccia. Retardation of the onset of turbulence by minor viscosity contrasts. *Phys. Rev. Lett.*, 87:174501, 2001.
- [28] C. Nouar and I. Frigaard. Stability of plane couettepoiseuille flow of shear-thinning fluid. phys. fluids 21 064104 (2009). *Phys. Fluids*, 21:064104.1–064104.13, 2009.
- [29] P. G. Drazin and W. H. Reid. Hydrodynamic stability. Cambridge University Press, 1995.